Techniques for Analysis of DSN 64-Meter Antenna Azimuth Bearing Film Height Records

R. Stevens, Chief Engineer
Telecommunications and Data Acquisition

C. T. Quach
Telecommunications Science and Engineering Division

The DSN 64-m antennas use oil pad azimuth thrust bearings. Instrumentation on the bearing pads measures the height of the oil film between the pad and the bearing runner. Techniques to analyze the film height record are developed and discussed. The analysis techniques present the unwieldy data in a compact form for assessment of bearing condition. The techniques are illustrated by analysis of a small sample of film height records from each of the three 64-m antennas. The results show the general condition of the bearings at DSS 43 and DSS 63 as good to excellent, and at DSS 14 as marginal.

I. Introduction

This report describes analyses of film height records of the DSN 64-m antenna azimuth thrust bearings. The 64-m antennas use an oil film hydrostatic azimuth bearing to support the 6.5-million-pound rotating weight of the alidade and tipping structure. The bearing configuration has a large oil pad at each apex of the triangular-shaped alidade base. Figure 1 shows the antenna and the azimuth bearing arrangement. The bearing pads have instrumentation to measure and record the height of the oil film between the pad and the supporting runner during operation of the antenna.

Film height records from each of the three antennas have been analyzed. Each record was analyzed in two ways: (1) calculation of the mean, standard deviation about the mean, and population histogram of the film height; (2) calculation and examination of the film height versus angular frequency spectrum. Also, averaged values of film height parameters versus azimuth angle have been developed for DSS 14. The analyses, which greatly compress the data on the records, imply the present and previous health of the bearings: good to excellent at DSS 43 (Australia) and DSS 63 (Spain); marginal at DSS 14 (Goldstone). The film height spectra clearly show the effects of the 11 regularly spaced bearing runner segments and provide quantitative assessment of the film height fluctuations resulting from the runner joints.

The analysis techniques used are simple in concept but laborious to apply with present equipment. The DSN plans to install equipment to produce digital film height records directly and to provide modest on-site data reduction capability. The equipment will be installed at DSS 14 in May 1983,

and at DSS 43 and DSS 63 in the fall of 1983. When that has been done, the techniques will be inexpensive and practical to apply and will be useful for support of operations and for maintenance planning of the bearings.

In the following, we present in order: the methods of taking and preparing the bearing film height data records, the techniques for data analysis, and the results of the analyses of the three antenna bearings. We close with suggestions on further development and application of the film height analysis techniques.

II. The Method of Taking and Preparing Film Height Records

A. Taking the Records

Each of the three bearing pads has precision linear transducers mounted to its periphery. The transducers are set to zero when the pad is sitting on the bearing runner. When the bearing is floated by oil supplied to recesses in the pads, the transducers measure the height, at their location, of the pad above the runner surface. The height is typically 0.005 to 0.010 in. for a properly operating bearing. The most heavily loaded pad, the rear pad (designated pad 3), has eight transducers as shown in Fig. 2; the other two pads have a transducer at each corner.

Film height records are customarily made from pad 3. Records are made several times each year. The transducers are connected to provide a voltage proportional to displacement; the voltage moves a stylus on a multichannel strip chart recorder. A normal recording has a calibrated trace from each of the eight transducers on pad 3. The azimuth position of the antenna is indicated by pips on the chart at 1° intervals as the antenna rotates, and the chart paper runs, at approximately constant speeds. A data run consists of a transducer zero calibration, a 360° rotation of the antenna, and a final transducer zero calibration. The run produces a chart 1/2 meter wide and 6 meters long. It is dated and annotated. The instrumentation is evidently accurate and stable within ≃0.0002 in.

B. Preparing the Data for Analysis

The traces were read and recorded by hand. Normally, five film height traces were read – from the transducers at the four corners and at the right center of the pad. They were read at 1° azimuth increments, to an accuracy of ≈±0.0002 in. of film height. The process takes about 20 hours per record; 11 records were read – four each from DSS 14 and DSS 43, and three from DSS 63.

III. The Methods of Data Reduction and Analysis

Correlation and spectrum analysis techniques have been used for solving problems and analyzing data in many fields of engineering. Here we calculate the autocorrelation function of the film height versus azimuth data and then obtain the power spectrum of the film height by Fourier transform. That is a standard procedure.

A conventional electrical waveform is voltage as a function of time and the related power spectrum is in units of watts per unit of frequency. In our case, the coordinates are film height as a function of azimuth rotation. Thus, the unit of spectrum power is film height squared, and the frequency is cycles of film height variation per azimuth revolution. The purpose in obtaining the spectrum of the film height is to provide for convenient examination of periodicities and other frequency characteristics of the data.

Histograms of film heights versus frequency of occurrence and the mean and the standard deviation about the mean of the film height are calculated. These, too, are standard calculations.

The power spectrum contains no phase information, so it cannot identify a characteristic associated with a particular azimuth angle. To do that, we return to the film height versus azimuth angle data and calculate azimuth-dependent film height parameters.

The details of the calculations and some sample results are presented in the following paragraphs.

A. Calculation of the Autocorrelation Function of Film Height

The autocorrelation function $C_{ff}(\gamma)$ is defined by:

$$C_{ff}(\gamma) = \lim_{T\to\infty} \frac{1}{2T} \int_{-T}^{T} f(\theta) f(\theta+\gamma)\, d\theta \qquad (1)$$

which is reformulated for our computational purpose as:

$$C_{ff}(N\Delta\theta) = \frac{1}{360} \sum_{\theta=1}^{360} f(\theta) f(\theta + N\Delta\theta) \qquad (2)$$

where $\Delta\theta = 1°$, $N = 1, 2, \ldots, 360$, and $f(\theta)$ is film height ($\times 10^{-3}$ in.).

The set of data f is reduced to zero mean before using Eq. (2) for computation.

1. **The computer program.** The program used to calculate the autocorrelation function of Eq. (2) was written in BASIC for the Hewlett Packard HP-85 computer used for the computations; it is given as a flow chart in Appendix A. The program reads the data file, then creates a new file which stores the computed autocorrelation data. Notice that it is necessary to compute only 180 points instead of 360 points for Eq. (2) (i.e., $C_{ff}(N\Delta\theta)$ is symmetric in N about every integral multiple of 180°); however, the subprogram is consistent with Eq. (2). That means the program will compute 360 points; the resulting autocorrelation function will be mirror imaged about $\theta = 180°$

2. **Sample results.** A sample result of the calculation of the autocorrelation function by the BASIC program implementation of Eq. (2) is given in Fig. 3. It is for the right-center probe data of DSS 43 taken in October 1978. $C_{ff}(N\Delta\theta)$ is plotted in terms of $N\Delta\theta$. According to Eq. (2), $N\Delta\theta$ is in units of degrees and $C_{ff}(N\Delta\theta)$ is in units of square inches ($\times 10^{-6}$).

B. Calculation of the Power Spectrum of Film Height

Applying the Fourier transformation to the autocorrelation function will produce the power spectrum function. The purpose of doing this is to achieve a function in the frequency domain. Consider the finite Fourier series:

$$f(\theta) = a_0 + \sum_{i=1}^{M} a_i \cos \frac{2\eta i\theta}{T} + b_i \sin \frac{2\eta i\theta}{T} \qquad (3)$$

where

$$a_0 = \frac{1}{T}\int_0^T f(\theta)\, d\theta$$

$$\left.\begin{aligned} a_i &= \frac{2}{T}\int_0^T f(\theta) \cos \frac{2\eta i\theta}{T}\, d\theta \\ b_i &= \frac{2}{T}\int_0^T f(\theta) \sin \frac{2\eta i\theta}{T}\, d\theta \end{aligned}\right\} \quad i = 1, \ldots, M.$$

In our case of application, $C_{ff}(N\Delta\theta)$ is $f(\theta)$ in the above a_i and b_i. Furthermore, $T = 360°$ and $M = 180°$, and one can write:

$$a(i) = \frac{1}{180} \sum_{i=0}^{180} \sum_{j=1}^{360} C_{ff}(j) \cos(i*j) \qquad (4)$$

$$b(i) = \frac{1}{180} \sum_{i=0}^{180} \sum_{j=1}^{360} C_{ff}(j) \sin(i*j) \qquad (5)$$

Finally, the film height power spectrum function, the Fourier transform of the autocorrelation function, is given by:

$$C(i) = [a(i)^2 + b(i)^2]^{1/2} \qquad (6)$$

1. **The computer program.** Equations (4), (5), and (6) are implemented in the program flow charted in Appendix B. The main program will input the autocorrelation data file and create the spectrum function file which is used to store the computed data.

2. **Sample results.** A sample result of the calculation of the film height power spectrum is shown in Fig. 4. It is for the right-center probe data of DSS 43 taken in October 1978. It is the power spectrum derived from the autocorrelation function of Fig. 3. In Fig. 4, the horizontal axis is the frequency of film-height variation for a revolution around the runner. The vertical axis is film height squared ($\times 10^{-6}$ in.^{2}) per cycle per azimuthal revolution (CPR).

The integral of the Fig. 4 power spectrum over a full azimuth rotation (360°) is 1.92×10^{-6} in.^{2}, which is identical to the value of the autocorrelation function at $N = 0$ in Fig. 3. This is a formal identity displaying selfconsistency of the calculations of the two computer programs.

An eleven CPR fundamental with harmonics out to the 6th are prominent features of the spectrum in Fig. 4. There are eleven segments in the azimuth bearing runner.

C. Calculation of the Histogram, Mean, and Standard Deviation of the Film Height

The purpose of generating a histogram is to show the distribution of the film-height data. A broad distribution of the film-height data means a large variation in film height. The mean, $\bar{h}$, and standard deviation about the mean, σ, of the data are important parameters of the distribution of film heights.

1. **The computer program.** The computer program used to generate histograms is in the Hewlett Packard HP-85 Standard Pac software. The program is written in BASIC and consists of 315 lines. It will input a specified data file from the tape and automatically sort the values into intervals or bins of equal width. Then a histogram and cell statistics can be generated and printed out at the user's request.

Two changes have been made in the program to fit our application. The size of the declared array has been changed

to the size of the data set that is used to produce the histogram. Also, a few lines of codes have been added to the cell statistics subroutine to print out the mean and the standard deviation of the sample data.

For further information and a listing of the program, refer to the documentation of Histogram Generator in the Hewlett Packard HP-85 Standard Pac.

2. **Sample results.** Figure 5 is a sample histogram. It is for the right-center probe of DSS 43 taken in October 1978. The horizontal axis is film height in inches $\times 10^{-3}$. The left side of the vertical axis gives the numbers of observations, and the right side of the vertical axis gives the percent of relative frequency.

The printed output on Fig. 5 gives the mean $\bar{h}$ and the standard deviation σ as 10.70 and 1.38 $\times$ 10^{-3} in., respectively. The histogram of Fig. 5 resembles a Gaussian distribution. Let us examine that. The values $\bar{h} \pm \sigma$, 2σ, and 3σ are:

	σ	2σ	3σ
$\bar{h}-$	9.31	7.93	6.55
$\bar{h}+$	12.08	13.47	14.85

Comparing the above with the cell statistics, the approximate number of film height samples (i) outside of the 1σ, 2σ, and 3σ about $\bar{h}$ is 118, 21, and 3, respectively. Thus, there is approximately 32.8 percent, 5.8 percent, and 0.8 percent of the samples outside of $\bar{h} \pm \sigma$, $\pm 2\sigma$, and $\pm 3\sigma$, respectively. For a true Gaussian distribution, the corresponding percentages are 31.7 percent, 4.6 percent, and 0.3 percent. That shows the distribution is, indeed, nearly Gaussian in character.

Finally, the value of the variance, σ^2, is 1.92 $\times$ 10^{-6} in.^{2}, which is identical to the value of the power spectrum integration and the value of the autocorrelation function at $N = 0$, as it must be. This again shows correctness of the procedure including the computer programs used.

D. Calculation and Plots of Compressed Film Height Parameters Versus Azimuth Angle

In addition to the spectral and statistical analyses, we need techniques for displaying and examining film height parameters related to a specific bearing azimuth angle. The display of the data must be compact, i.e., reduced from the 1/2 X 6 meter original record to a format perhaps the size of this piece of paper. To do that, we proceed as follows.

Consider the equation:

$$\bar{h}(\theta, W) = \frac{1}{W+1} \sum_{\theta_W = \theta - \frac{W}{2}}^{\theta_W = \theta + \frac{W}{2}} f(\theta_W) \qquad (7)$$

where θ_W is an integer; $\bar{h}(\theta, W)$ is the mean film height at azimuth θ, smoothed over the window W centered on θ; $f(\theta_W)$ is the film height data at azimuth θ_W. The smoothed film height $\bar{h}(\theta, W)$ from Eq. (7) can be displayed in a compact graphical form.

In the same way, other smoothed functions of the film height versus azimuth can be computed. e.g., $\sigma(\theta, W)$ and $\bar{h}/\sigma\ (\theta, W)$. These techniques are used to develop plots in Section IV.C.1 of this article.

IV. Results of Reduction and Analysis of Film Height Records From the 64-Meter Antennas

A sampling of film height records from the three antennas was reduced and analyzed using the techniques described in the preceding sections. The records are identified in Table 1.

Spectrum plots are shown of the film height power versus azimuthal angular frequency for the *right center*[1] probe data of each record. Film height statistics from the *four corner* probes of each record are given. Also, locally averaged azimuth-dependent film height parameters are calculated from two of the DSS 14 records.

The existing analytical design model of the bearing does not predict significant detailed behavior shown by analyses of the experimental film height data. Therefore, we give physical interpretations of some spectral and statistical results to help in future model development.

We first discuss the *set* of spectral and film height statistics data. Then, because each antenna bearing has a different film height signature, the interpretations of their data are discussed individually.

A. The Set of Film Height Power Spectra

The film height power spectra of the right center probe of pad 3 for the several records are displayed in Figs. C-1 through C-11 of Appendix C.

[1] Spectra of four corner probe data were also computed and analyzed; for brevity, that work is omitted from this article.

1. **Evidence of runner joint effects.** In all of the spectra, but to varying degree, there is evident an 11-CPR component with its higher harmonics (i.e., 22, 33, etc., CPR). The 11 joints, the only regular inhomogeneity in the runner, produce the fluctuation power (variance, σ^2, in film height) at the 11-CPR and harmonically related frequencies.

2. **Significance of runner joint effects.** We can illustrate the relative significance of the bearing segment joints in the total variance of the bearing film height. Figures 6(a), (b), and (c) show plots of the total film height variance, which is the integral of the power spectra over the full range of azimuthal frequencies, excepting zero. Those figures also show the variance due to the power contribution at 11, 22, 33, etc., CPR. The relative contribution of the bearing joints to the total film height variance is quite different for each antenna; the differences are qualitatively evident from the spectra of Appendix C.

Further discussion of the spectrum plots of the individual antennas will be given in Section IV.C.

B. The Set of Film Height Statistics

Histograms, and values of the mean, and the standard deviation about the mean of the film height data were computed for the set of records given in Table 1. (The DSS 43 record of March 1982 was not included because, at that particular time, one of the four corner probes was defunct.) The results were in the format shown in Fig. 5.

1. **Comparison of statistics with Gaussian model.** In Section III.C.2 on Analysis Methods, we observed that the distribution of film height data is Gaussian-like. Table 2 addresses that proposition for the complete data set of 14,400 points; it is derived from the calculation of mean heights and standard deviations as shown in Fig. 5.

Referring to Table 2, the percentage of samples within the mean ±1, 2, and 3 standard deviations is generally close to that of a Gaussian distribution. The table also shows the *actual* percentage of the 1440 film-height samples in each record which are *below* the value $\bar{h} - 3\sigma$. Note that, with the progress of time, the number of very low film heights is decreased, and the "wings" of the distribution are skewed – presumedly a result of maintenance shimming of the bearing to correct specific low film height areas.

2. **Condition of a bearing inferred from statistics.** The purpose in displaying the Gaussian-like distribution of the film height data is to develop a simple technique to show the general condition of the bearing from a film height record. That technique is displayed in Figs. 7(a), (b), and (c), which are plots of $\bar{h}$, and $\bar{h} \pm 3\sigma$ for the three bearings. Because of the approximate Gaussian distribution, there should be very few (~2) points with film height lower than $\bar{h} - 3\sigma$. Also shown on the figures are the *actual* lowest film heights taken from the records and the design, minimum normal operating, and minimum safe film heights in the bearing.

It is evident that analysis of a more complete set of historical records, e.g., annually, would provide a basis for a useful extrapolation into the future of the general condition of a bearing.

C. Discussion of Individual Antennas

As noted, the bearings of the three antennas have different individual film height characteristics. The interpretations of their film height spectra and statistics are discussed individually in the following paragraphs.

1. DSS 14 characteristics

a. Runner joint (11 CPR) components in spectra. The first two spectra (August 1971, July 1981; Figs. C-1 and C-2) clearly show power at the 11 CPR frequency of the bearing segments. In the two later spectra, Figs. C-3 and C-4, the 11 CPR components are not as clear although there is considerable power in the general regions around 11 CPR and related harmonics. That behavior is consistent with the variance plot of Fig. 6(a), which shows that the relative contribution of the 11 CPR and exact harmonic components in the two latest records (December 1981 and February 1982) is down by a factor of about 2 from the previous record (July 1981). It may be a coincidence, but several gaps of ~0.010 to 0.040 in. at the bearing joints were closed during bearing maintenance in November 1981.

b. Broadband components in spectra. There is broadband noise power out to 60-70 CPR in the film height spectra of all antennas. It is especially prominent in the DSS 14 spectra. We consider a model for the generator of that noise. The bearing pad is very stiff (20 × 40 × 60 in. solid steel); we would expect that faulty support of the bearing runner would produce film height variations that are correlated over an angular extent related to the pad dimension along the runner. A possible mechanism is depicted in Fig. 8.

The actual film height records show many randomly spaced fluctuations which resemble the little cosine wavelet of the sketch, both in shape and angular dimension.

The power spectrum shape of an idealized cosine wavelet one pad-length long is as shown in Curve A of Fig. 9. It is superimposed on the February 1982, DSS 14 spectrum of Fig. C-4. The shape of the wavelet spectrum resembles the envelope of the film height spectrum above about 20 CPR.

For comparison, the spectral shapes are shown for film height wavelets which are one-half and twice the length of the pad (Curves B and C, respectively).

c. Low frequency components in spectra. Another distinguishing characteristic of the DSS 14 spectra is the large peaks in the 1-3 CPR range. One might suspect that the spectral analysis process is producing artifacts for frequencies so close to zero. To examine that, we return to the original film height records. Figure 10 shows the actual right center probe film height versus trough azimuth for the August 1971 DSS 14 record. In that figure, the one sample per degree data have been smoothed over a 20° wide azimuthal window. Otherwise, the data are as taken from the original record. The record has a readily discernible 1 CPR variation, qualitatively consistent with the spectrum plot. To further illustrate that consistency, we proceed as follows. The power in the prominent 1 CPR component of the August 1971 record (Fig. C-1) is $\approx 0.26 \times 10^{-6}$ in.^{2}. The amplitude of a 1-CPR sine wave of that power is:

$$A = \sqrt{2P} = \sqrt{2 \times 0.26 \times 10^{-6} \text{ in.}^2} = 0.72 \times 10^{-3} \text{ in.}$$

An approximate fit of a 1-CPR sine wave of that amplitude added to the average film height $\bar{h}$ is depicted in Fig. 10. It is qualitatively consistent with the original smoothed data. The possible cause of the very slow variations in film height with azimuth is not evident; the variations do, however, exist.

d. Search for the evidence of grout keyways in spectra. When this work was started, a principal purpose was to identify the effects of suspected faulty grout keyways under the DSS 14 bearing runner. There are 40 regularly spaced keyways under the bearing runner. They are formed by rectangular cavities in the top of the concrete pedestal. When the grout was originally placed between the runner and the pedestal, it was supposed to fill the cavities. It is known from coring samples that the filling was not uniformly sound. The purpose of the keyways is to lock the grout securely to the pedestal. We anticipated identifying the 40-CPR signatures in the film height spectra.

We did not find evidence of the keyways in any of the right center probe or four corner probe spectra. To further investigate the keyway matter, pad 3 was fitted with additional probes at the middle of its long dimension, see Fig. 11. It was expected that the probes at the centers of the long dimension of the pad would be most effective in detecting poor support of the runner above the 40-grout keyways. The February 1982 record has data from the new CF and CR probes. The spectra from that data *do not* show significant 40-CPR power (the spectral plots are not included here). This result, and the fact that the film height spectra of the four corner and right center probes also showed no 40-CPR power, leads us to the unexpected conclusion that the grout keyways are not significant systematic contributors to degraded performance of the DSS 14 bearing.

e. Investigating bearing support using new pad center probes. If the support under the bearing pad is compliant relative to the pad, the bearing runner will be most depressed in the middle of its long dimension. We should measure that effect by differencing the film height at a center probe and the average of the film heights at the two ends of the same face of the pad. This is, referring to Fig. 11:

$$\left(h_{CF} - \frac{h_{LF} + h_{RF}}{2}\right); \qquad \left(h_{CR} - \frac{h_{LR} + h_{RR}}{2}\right)$$

Plots of those differences versus trough azimuth, smoothed over ±10° in azimuth, are shown in Figs. 12 and 13. From those figures one is led to suspect that the support is better under the inner (rear) area of the bearing runner than it is at the outer (front) area, and that the region around 170° of trough azimuth is especially well supported. Only a single record with the new CF and CR probes has been analyzed; the results need further validation to ensure that they are authentic.

f. Right center versus corner probe film heights, DSS 14 compared with overseas antennas. The DSS 14 bearing has another special characteristic. Table 3 provides a comparison of the mean film height at the right center probe with the average of the four corner probes for the records of all antennas.

The DSS 43 and 63 bearings have equal or slightly greater mean film heights at the center probe compared to that at the four corner probes. All but the earliest record from DSS 14 show lower film heights from the right center probe. This may be a result of the extensive use of radially contoured shims under the bearing runner at DSS 14.

g. An examination of locally averaged film height and standard deviation. A high average film height $\bar{h}$ with a low standard deviation σ are the desired characteristics of a bearing. In Fig. 14, those parameters from the February 1982 DSS 14 record are plotted versus trough azimuth. They have been smoothed over ±10° in azimuth. Also, the quotient, $\bar{h}/\sigma\ (\theta)$, is plotted – the higher the $\bar{h}/\sigma\ (\theta)$ quotient, the better the bearing in the ±10° region around the associated azimuth value. The regions of trough azimuth over which a portion of the pad is over a runner joint are indicated in Fig. 14.

The presentation of Fig. 14 displays significant characteristics of the DSS 14 bearing. The average smoothed film

height, $h(\theta)$, is decent ($9.2 \pm 0.7 \times 10^{-3}$ in.). There are some rather large areas between the joints where the $\sigma(\theta)$ is good ($\sigma < 1.7 \times 10^{-3}$ in.). The poor areas are clearly shown by the $\bar{h}/\sigma$ (θ) plot; they are systematically associated with the runner joints. Finally, all of the plots are distinctly mirror-imaged about a trough azimuth of 162°. The mirror imaging is especially evident in the $\bar{h}/\sigma$ (θ) plot; the cause is at present a mystery.

2. DSS 43 characteristics

a. Runner joint (11-CPR) components in spectra. The dominant features of the DSS 43 spectrum plots (Figs. C-5, 6, 7, and 8) are the 11-CPR component and its harmonics. As presented in Fig. 6(b), a large fraction of the total film height fluctuation power is contained in those components.

Plots of the power in the 11-CPR components taken from the earliest (September 1976) and the latest (March 1982) record spectra are depicted in Fig. 15. The characters of the two other record spectra (October 1978 and June 1980) generally lie between the two shown. The basic shape of the spectrum has not changed substantially in the 6 years between the records, but the power in each component has increased considerably; e.g., the 11-CPR fundamental ($n = 1$ in Fig. 15) has almost doubled in power. Evidently some changes have occurred over the years in support under the runner joints or the continuity of the joints, or both.

b. Model of joint-dominated film height fluctuations, DSS 43. By studying the original film height records and doing some trial-and-error spectrum shape fitting, we synthesized the very simplified film height wave shape shown in Fig. 15. The value of $\theta_1 = 3.74°$ in the model is the angular half width of the bearing pad. The 32.7° long pattern repeats 11 times in one azimuth revolution, corresponding to the number of runner joints. The ratio $a_2/a_1 = 0.3$ is representative of the average behavior of the experimental film height data in the vicinity of the joints. The amplitude $a_1 = 2.1 \times 10^{-3}$ of the model waveform was used to put its spectrum between the two experimental spectra. To closely match the September 1976 record, select $a = 1.7 \times 10^{-3}$ in.; to match the March 1982 record select $a_1 = 2.4 \times 10^{-3}$ in. The actual experimental film height data do not have the sharp corners of the model wave form but rather the smooth contours of the cosine wavelet. However, that difference only modestly affects the higher order component powers, not the dominant lower order ($n = 1, 2$) components; the simple model was used for ease of calculation.

The model displays a persistent lower film height in the vicinity of the runner joints; that is what produces the large 11-CPR fundamental frequency component in the spectra. The spectra show that the magnitude of this effect has increased with time. The physical cause, to our knowledge, is not now known. Although the bearing appears to be in good condition, this characteristic should be understood in the context of its long-term maintenance. Abrupt steps at the runner joints are not much in evidence at DSS 43, either in the raw data or in the derived spectra. Therefore, they were not included in the model. One should remember that the fluctuation model waveform (cf Fig. 15) "sits" upon a healthy mean film height of 9 to 10 thousandths of an inch.

c. Broadband components in spectra. In Fig. C-8, the DSS 43 broadband noise can be compared with the spectral envelope of 1- and 2-pad-length-long cosine wavelets. The shape of the bearing noise spectrum appears to lie between those of the two models.

3. DSS 63 characteristics

a. Runner joint (11-CPR) components in spectra. The DSS 63 spectrum plots (Figs. 3-9, -10, and -11) show power at the 11-CPR fundamental and its harmonics. The power is distributed to the higher harmonics more so than in the DSS 43 spectra; it is visible out to the 8th harmonic (88 CPR).

Plots of the power in the 11-CPR components from the spectra of the earliest (July 1973) and the latest (March 1982) records are depicted in Fig. 16. The character of the other record spectrum (June 1978) generally lies between the two shown. The shape of the spectrum has changed noticeably, and its magnitude, while still relatively small, has increased in the 8-1/2 years between the records. By examination of film height spectra at one- to two-year intervals in the future, any significant progress of deterioration of the joint support or continuity can be identified.

b. Model of joint-dominated film height fluctuations, DSS 63. Again by studying the original film height records and doing trial-and-error spectrum shape fitting, we prepared a simple model for the periodic film height waveform (cf Fig. 16). The parameters of the model were selected so that its spectrum envelope lies within that of the two data records shown. It is very similar to that of the June 1978 record, not shown. Increasing τ (cf Fig. 16) brings the model toward the March 1982 record spectrum; decreasing τ brings it toward the July 1973 record spectrum. This relates to a slow degradation of pad support in the joint regions versus the support at the regions midway between the joints.

The DSS 63 model has a relatively modest amplitude. The humped valley around the joints is broad with an average height not far below that of the plateau between the joints. The narrow downward triangular spikes at the joints mimic abrupt 0.001- to 0.002-in. steps displayed at most of the

joints in the DSS 63 film height records. These rapid variations produce the higher harmonics ($n = 6, 7, 8$) in the DSS 63 spectra.

c. Narrowband components (besides 11 CPR) in spectra. The DSS 63 spectra (Figs. C-9, 10, and 11) consistently show power at 9 CPR, 38 CPR, and 90 CPR. Added together, those components contain 6 percent, 17 percent, and 15 percent of the total fluctuation power, σ^2, in the July 1973, June 1978, and March 1982 spectra, respectively.

The 9-CPR component in the June 1978 record is the largest of the set at 0.14×10^{-6} in.^{2}. That corresponds to a 9-CPR sine wave of peak-to-peak amplitude $2a = 2\sqrt{2P} = 2\sqrt{2 \times 0.14 \times 10^{-6} \text{ in.}^2} \cong 1.1 \times 10^{-3}$ in., which is neither negligible nor really significant. We have no postulation on the source of the 9, 38, or 90-CPR spectral components.

d. Broadband components in spectra. In Fig. C-11, the DSS 63 broadband noise and the 1-pad-length cosine wavelet spectral shapes are compared. There is qualitative agreement, indicating consistency with a model of the type depicted in Fig. 8.

V. Discussion

Our conclusions from analyses of the several bearing records is that the spectral and statistical analyses techniques can provide reliable information on the previous and present conditions of a bearing. Because the results appear consistent, not erratic, over long time spans, useful extrapolation to future bearing condition should be available using the methods. The spectral analysis and azimuth-related film height parameter analysis also provide systematic pointers to guide investigation of specific existing or incipient faults in the bearings.

The methods get the voluminous data from the film height records into a form which can be digested and preserved and can be usable for comparisons over long time spans. Fundamentally, the results are easy to obtain and, with familiarity, easy to interpret.

Analysis of additional historical records, and those currently being obtained, requires the laborious reading of the analog strip chart traces. However, that is just painful, not really very expensive or time consuming. Within a year, when the current plans are carried through, the analog recording equipment will be replaced with digital equipment. The digital records then obtained will be in a form to directly input the analysis programs we have used.

A. Regarding the Statistical Analyses

The mean film height $\bar{h}$ and standard deviation about $\bar{h}$, σ, of the four corner probes appear to be meaningful measures of the general condition of a bearing. If a reasonable number of the historical records (e.g., two or three per year to reduce environmental effects) were analyzed, we expect that a useful extrapolation of future bearing maintenance needs would result. The calculations and interpretation of the results are especially straightforward.

B. Regarding the Spectral Analyses

The spectra derived faithfully display the systematic nature of the film height fluctuations and in a way that cannot be gleaned from studying the noncompressed raw data. The spectral analysis process can be useful in developing improved analytical models of the actual bearing performance (models which produce the experimentally observed behavior), and in assessing the results of maintenance work on the bearings.

A particular extension of the spectral analyses, which we expect would contribute to understanding the bearing operation, is the calculation of the *cross*-correlation and *cross*-spectra of the film heights at the two ends of the pad. In the model we discussed in the article to produce the cosine wavelet fluctuation from the right end probe, there should be produced simultaneously in azimuth a companion wavelet from the left end probe. The cross-correlation/cross-spectrum will quantitatively display that characteristic and thus support (or invalidate, or revise) the model. The raw data suggest the wavelets from the two pad ends do indeed occur at times simultaneously, as predicted by the model. This work is being planned.

C. Regarding the Calculation of Compressed Film Height Parameters Versus Azimuth Angle

With the data prepared for the statistical and spectral analyses, it can be easily manipulated to display in compressed form various film height parameters as a function of trough azimuth. We illustrated that, for example, with plots of locally averaged $\bar{h}(\theta)$, $\sigma(\theta)$, and the quotient $\bar{h}/\sigma(\theta)$. In that form, the film height data can be readily compared with other measured or calculated azimuth-related parameters of the bearing installation, e.g., with pedestal concrete modulus, to identify correlations.

In particular, we suggest that additional records of the new center front and rear probes at DSS 14 be analyzed. That will improve understanding of the bearing runner support as a function of azimuth and also across the width of the bearing (radially).

Reference

1. *The NASA/JPL 64-Meter-Diameter Antenna at Goldstone, California: Project Report*, Technical Memorandum 33-671, Jet Propulsion Laboratory, Pasadena, Calif., July 15, 1974.

Acknowledgments

I. D. Wells and W. H. Kuehn provided the records we analyzed. F. D. McLaughlin provided the antenna and bearing sketches. Discussions with M. S. Katow, H. D. McGuinness, F. D. McLaughlin, H. P. Phillips, A. A. Riewe, and I. D. Wells have been helpful in understanding engineering features of the bearing and its instrumentation.

Table 1. Film height records analyzed

(Each record is from the antenna rear pad, no. 3)

Antenna	Date recorded	Comment
DSS 14	08/27/71	Earliest record available
DSS 14	07/05/81	Prior to bearing fault of 9/81
DSS 14	12/02/81	After bearing fault rework
DSS 14	02/04/82	Includes probes at front and rear pad centers
DSS 43	09/21/76	
DSS 43	05/10/78	
DSS 43	06/11/80	
DSS 43	03/31/82	Only 3 of 4 corner probes available
DSS 63	07/25/73	
DSS 63	06/14/78	CW Az rotation (all above use CCW)
DSS 63	03/06/82	CW Az rotation

Table 2. Distribution of film heights at four corner probes, comparison with Gaussian distribution

Data	Percentage of samples within			Percentage of samples
	$\bar{h} \pm \sigma$	$\bar{h} \pm 2\sigma$	$\bar{h} \pm 3\sigma$	Below $\bar{h} - 3\sigma$
Gaussian model	68.3	95.4	99.7	0.13
DSS 14 records:				
August 1971	68.2	94.9	99.3	0.56
July 1981	64.9	94.0	99.5	0.06
December 1981	64.3	96.2	99.7	0.08
February 1982	65.7	96.1	99.6	0.00
DSS 43 records:				
September 1976	64.2	93.5	99.7	0.25
October 1978	64.1	95.3	99.9	0.00
June 1980	64.8	96.5	99.9	0.00
DSS 63 records:				
July 1973	67.8	96.5	99.6	0.34
June 1978	65.9	94.3	99.4	0.21
March 1982	66.9	95.7	99.6	0.05
Average, all records				
(14,400 samples)	65.7	95.3	99.6	0.15

Table 3. Comparison of mean film heights of right center and four corner probes ($\bar{h}$ in in. $\times 10^{-3}$)

Record	$\bar{h}$ Right Center	$\bar{h}$ Four Corners
DSS 14, August 1971	10.4	8.2
DSS 14, July 1981	6.4	7.3
DSS 14, December 1981	7.5	9.4
DSS 14, February 1982	7.6	9.2
DSS 43, September 1976	10.7	10.5
DSS 43, October 1978	10.7	10.3
DSS 43, June 1980	11.8	11.3
DSS 63, July 1973	11.2	10.5
DSS 63, June 1978	11.1	10.9
DSS 63, March 1982	11.2	11.2

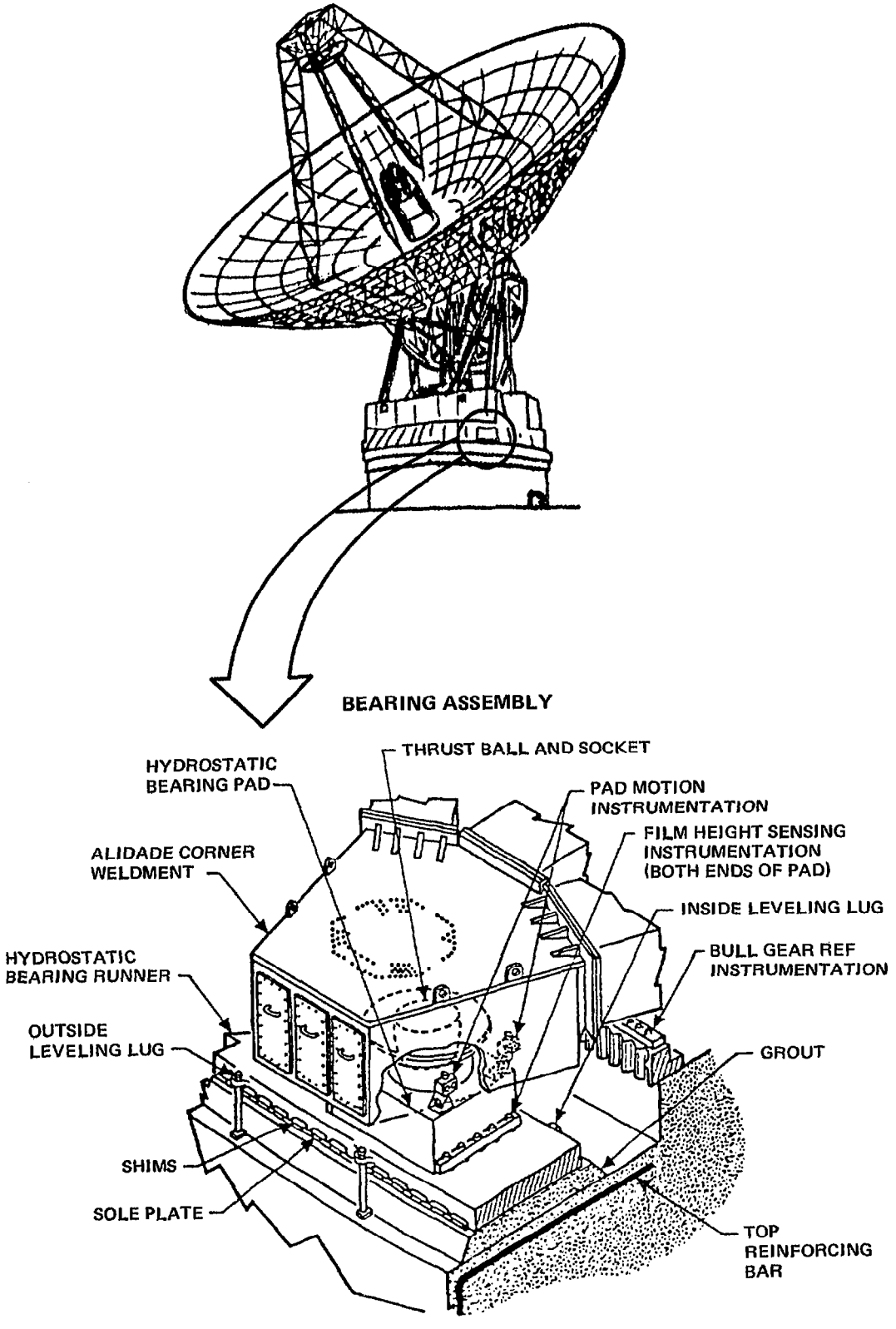

Fig. 1. 64-meter antenna showing azimuth thrust bearing arrangement

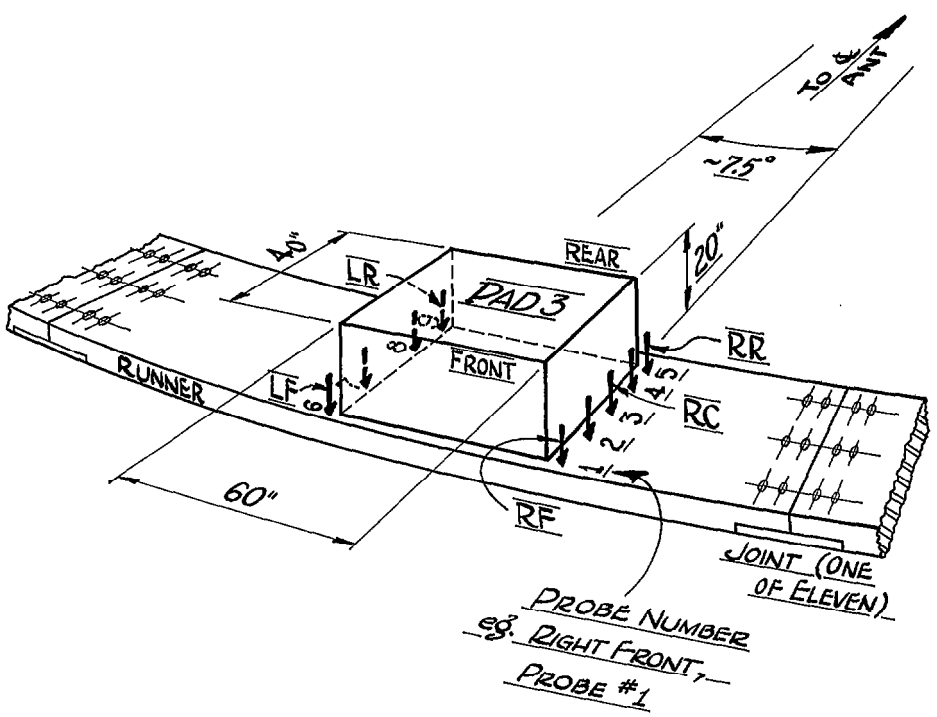

Fig. 2. Azimuth bearing pad with film height transducers

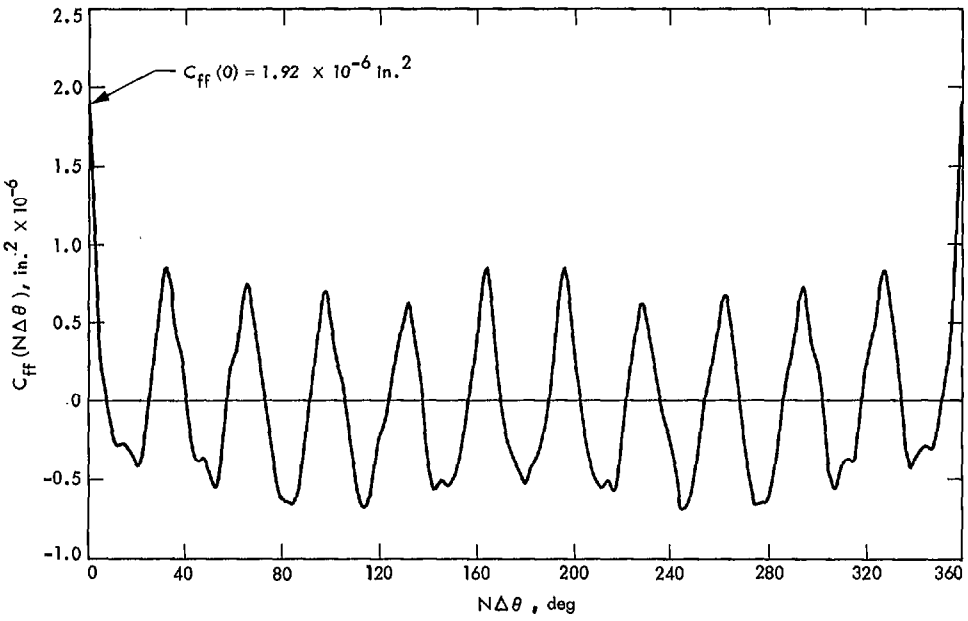

Fig. 3. Autocorrelation of film height; right center probe. DSS 43, October 1978

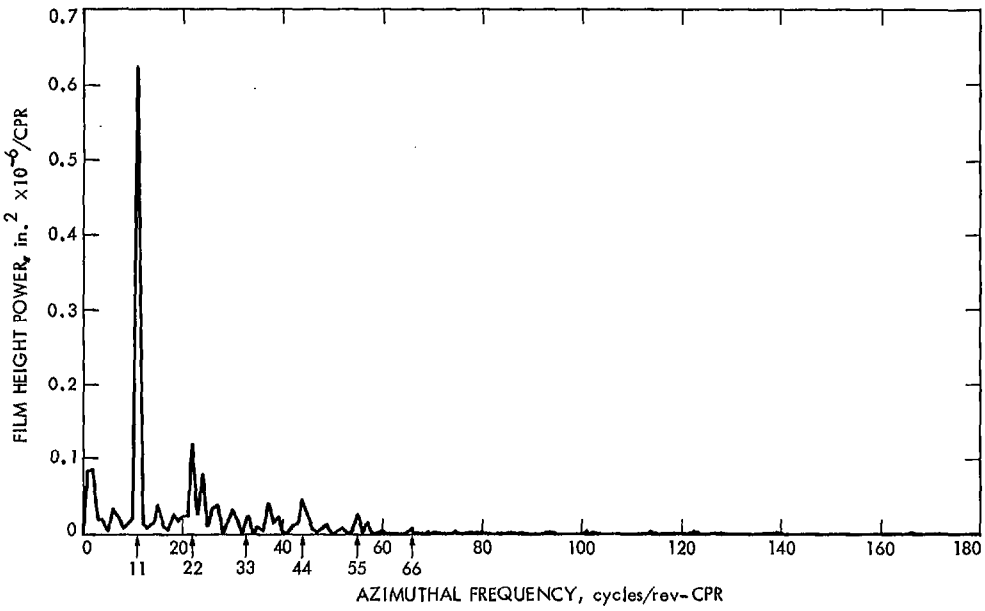

Fig. 4. Power spectrum of film height; right center probe. DSS 43, October 1978

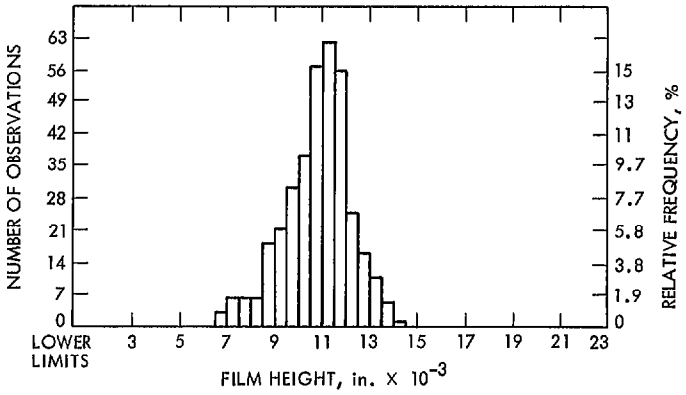

CELL WIDTH = 0.5 X 10^{-3} in.

CELL STATISTICS

CELL #	LOWER LIMIT	NUMBER OF OBSERVATIONS	RELATIVE FREQUENCY
8	6.50	3	0.83
9	7.00	6	1.67
10	7.50	6	1.67
11	8.00	6	1.67
12	8.50	18	5.00
13	9.00	21	5.83
14	9.50	30	8.33
15	10.00	37	10.28
16	10.50	57	15.83
17	11.00	62	17.22
18	11.50	56	15.56
19	12.00	25	6.94
20	12.50	16	4.44
21	13.00	11	3.06
22	13.50	5	1.39
23	14.00	1	0.28

THE MEAN OF THE SAMPLE, $\bar{h}$, IS:
10.7 X 10^{-3} in.

THE STANDARD DEVIATION ABOUT THE MEAN OF THE SAMPLE, σ, IS:
1.38 X 10^{-3} in.

Fig. 5. Histogram and cell statistics of right center probe film height. DSS 43, October 1978

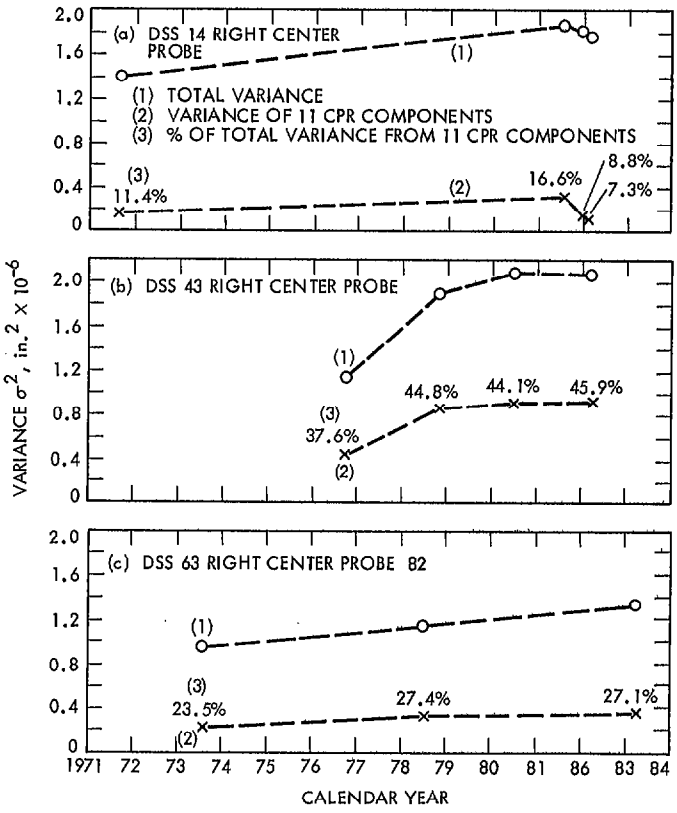

Fig. 6. Total variance and variance from 11-CPR components of film height

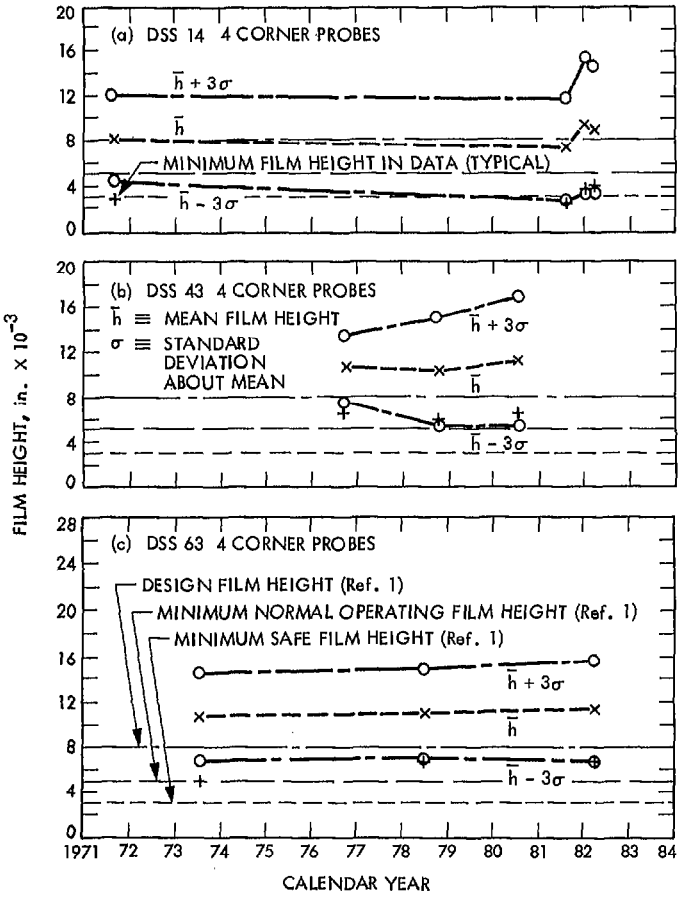

Fig. 7. Mean and mean ± three standard deviations of film height

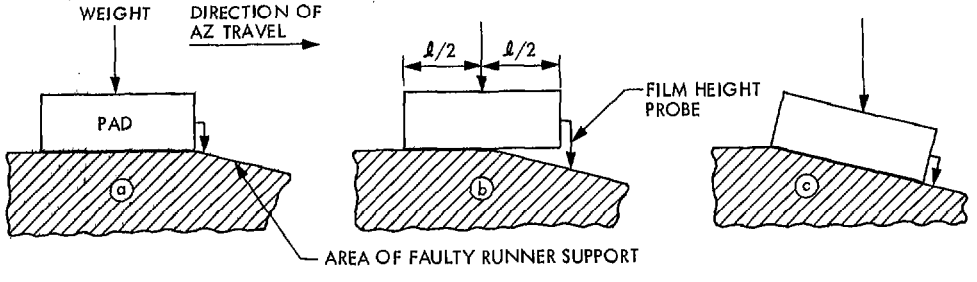

FRONT OF PAD MOVES OVER START OF SLOPE IN ⓐ AND ITS FILM HEIGHT INCREASES, ⓑ. AFTER LOAD CENTER MOVES OVER SLOPE EDGE, PAD SETTLES DOWN, ⓒ. THE EXPECTED FILM HEIGHT VARIATION AT THE LEADING EDGE PROBE IS DEPICTED IN ⓓ BELOW.

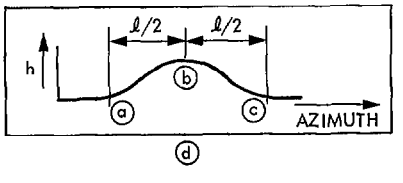

Fig. 8. Model of film height variation related to pad azimuth dimension

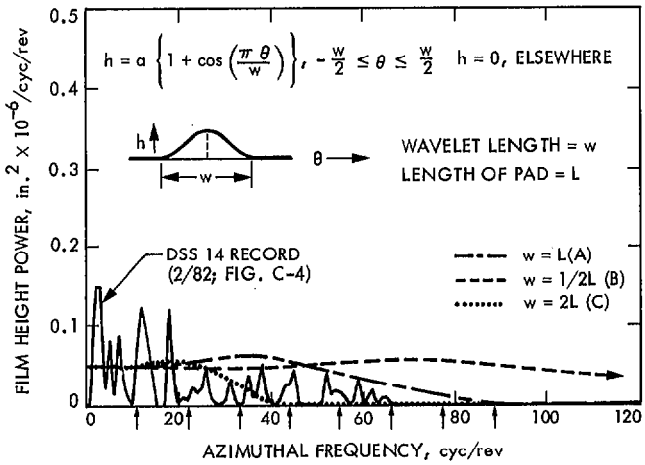

Fig. 9. Power spectra of model wavelets (with February 1982 DSS 14 spectrum)

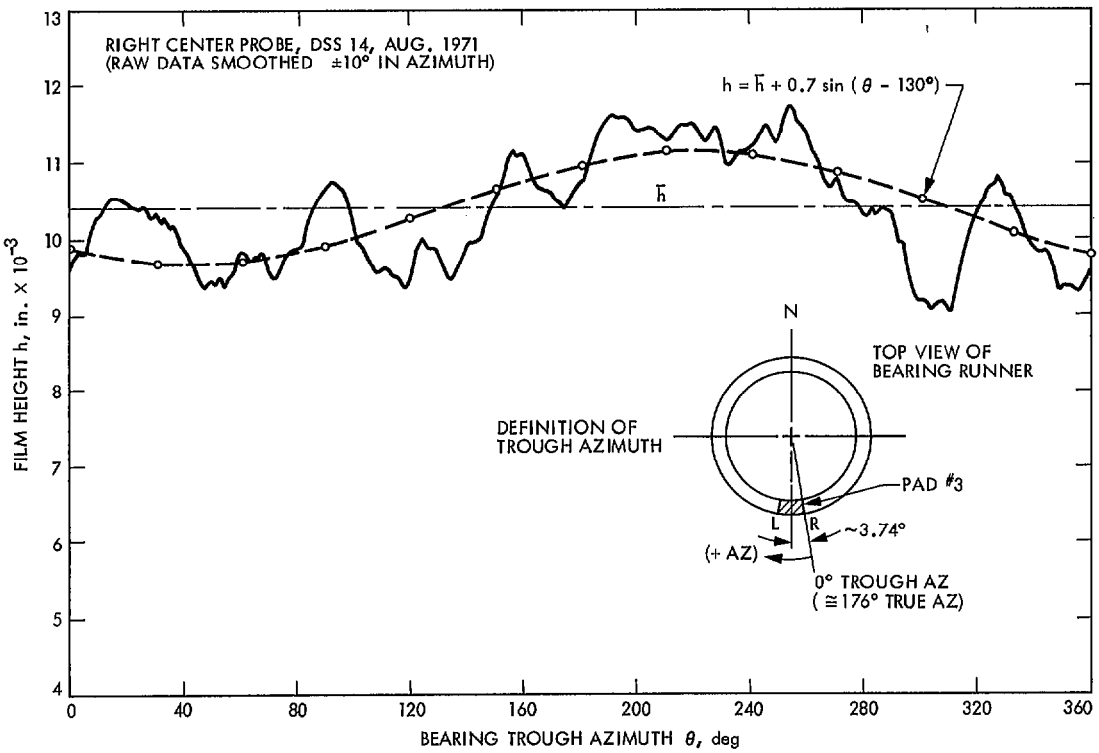

Fig. 10. Smoothed film height; approximate 2-CPR component

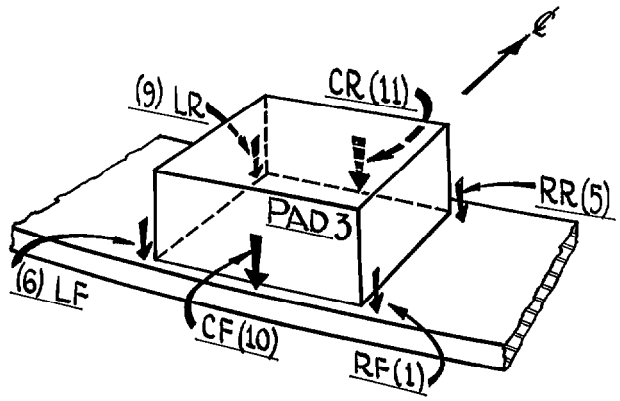

Fig. 11. Location of new center front (CF) and center rear (CR) film height probes on Pad 3, DSS 14

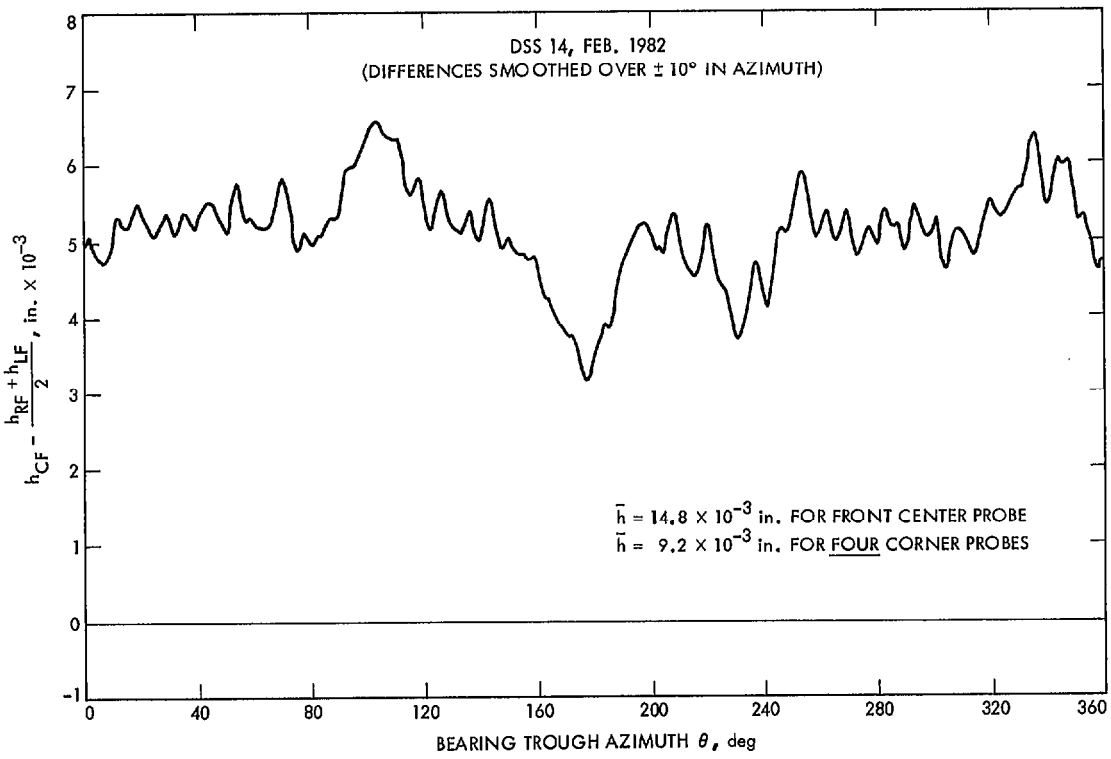

Fig. 12. Film height difference between front center and average of front end probes

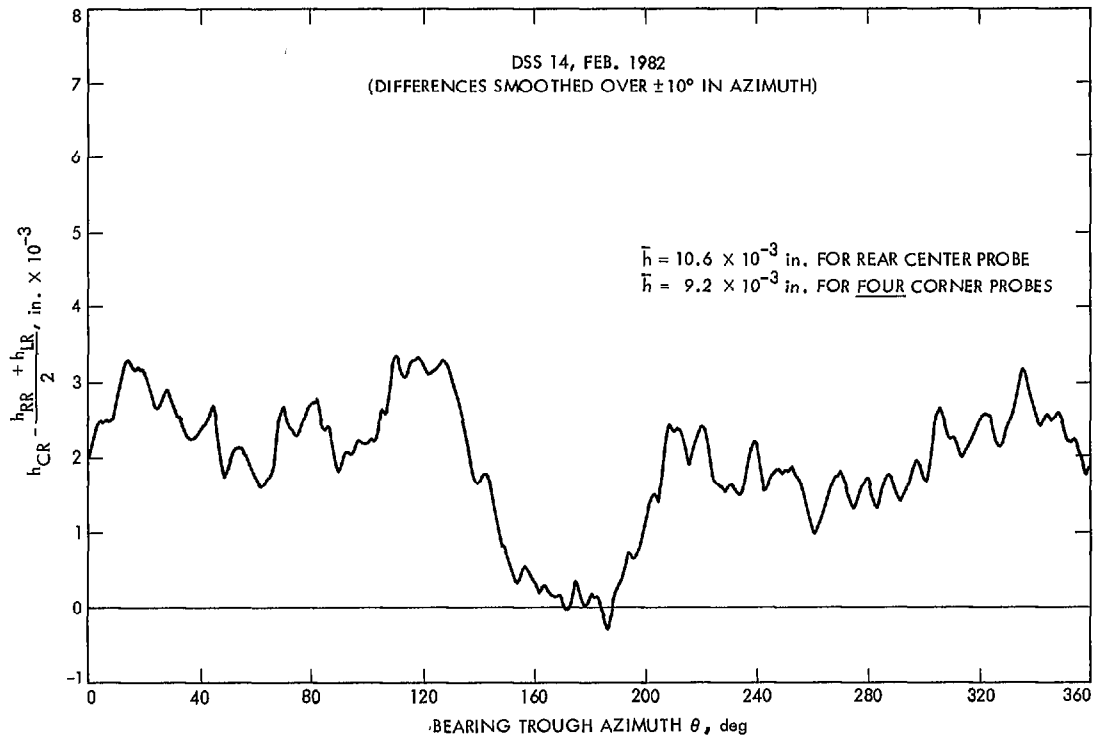

Fig. 13. Film height difference between rear center and average of rear end probes (DSS 14)

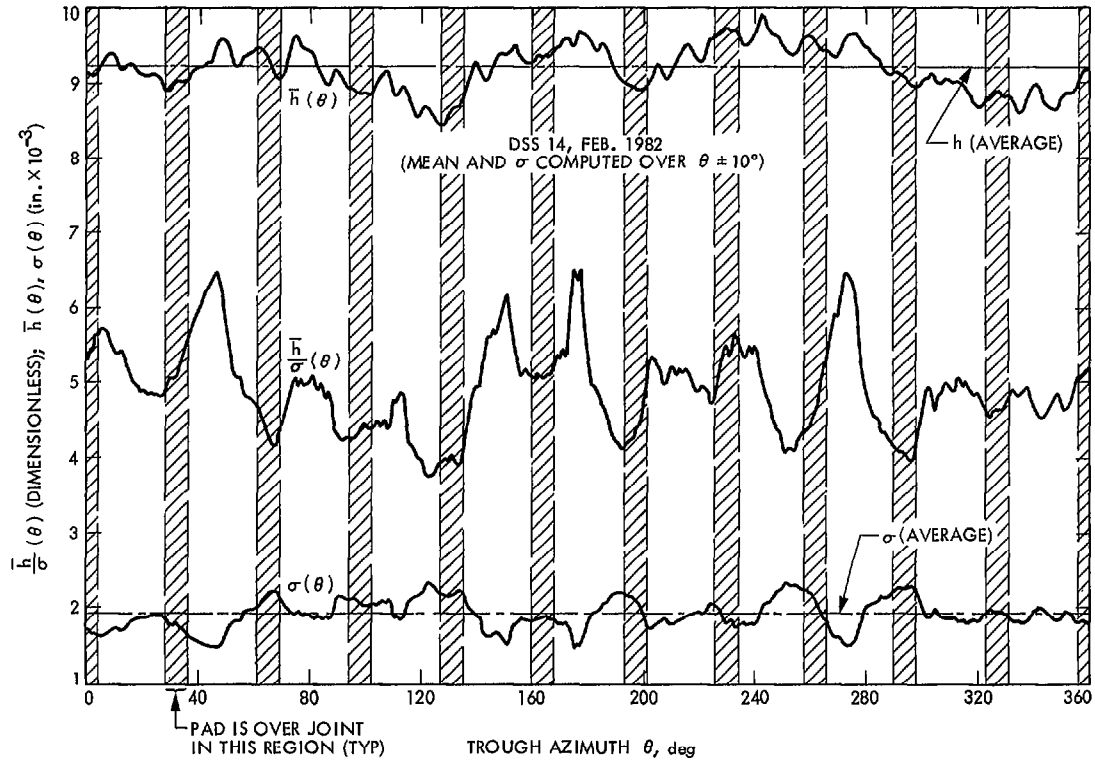

Fig. 14. Plots of local mean film height $\bar{h}(\theta)$, local standard deviation $\sigma(\theta)$, and their quotient $\bar{h}/\sigma(\theta)$ versus trough azimuth (four corner probes)

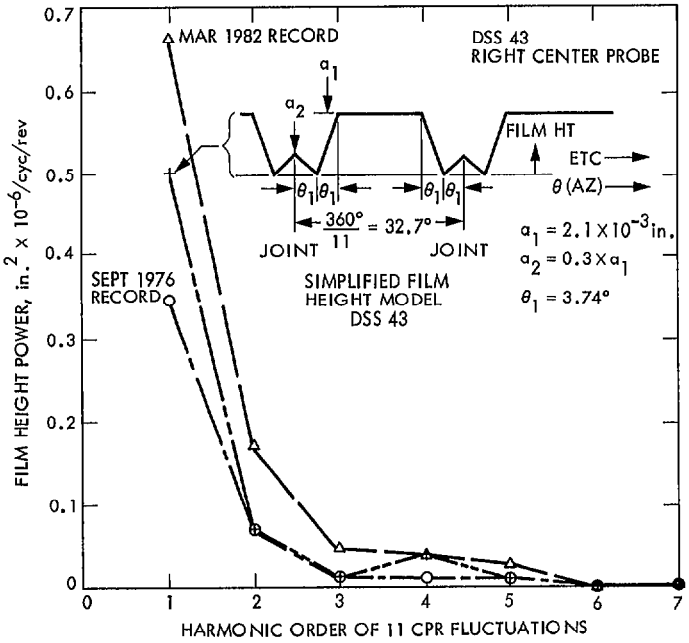

Fig. 15. Power in runner joint induced fluctuations and for simple film height model, DSS 43

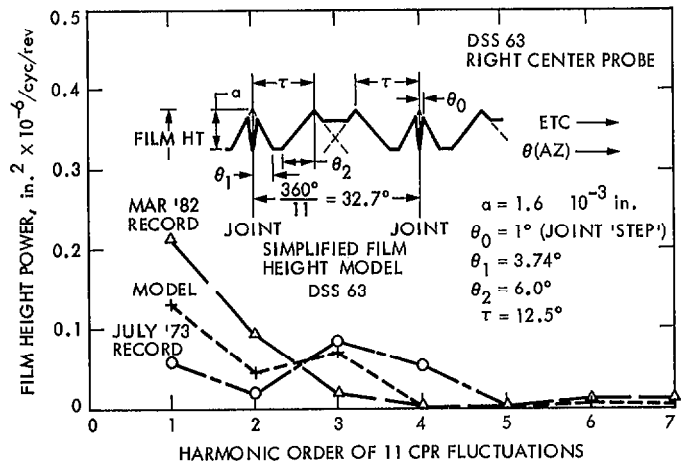

Fig. 16. Power in runner joint induced fluctuations and for simple film height model, DSS 63

Appendix A

Flow Chart for Calculation of Autocorrelation Function

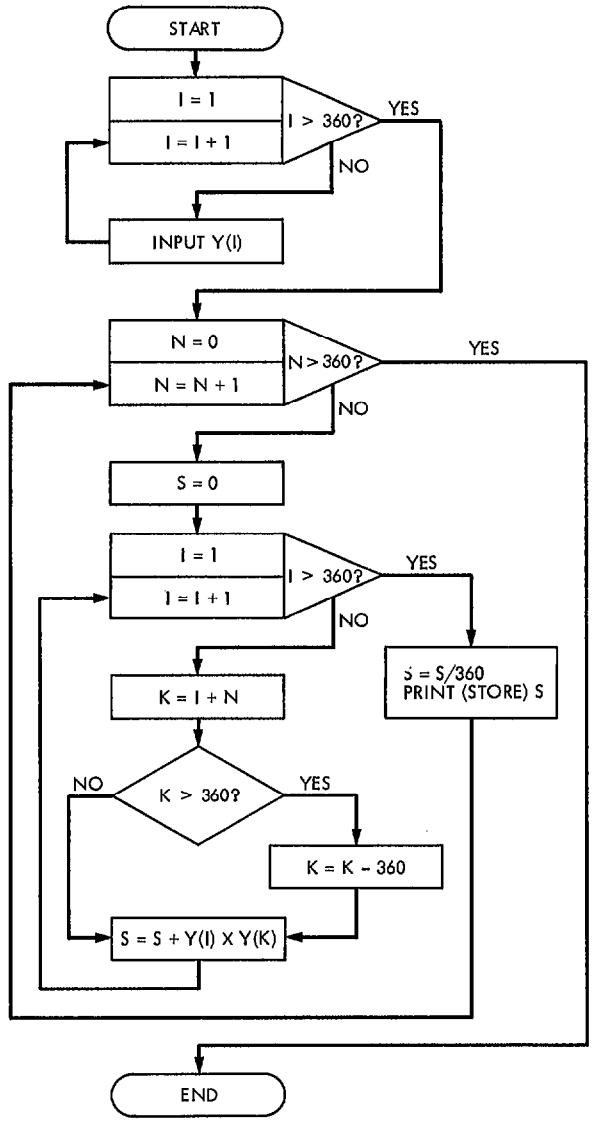

Appendix B

Flow Chart for Calculation of Power Spectrum from Autocorrelation Function

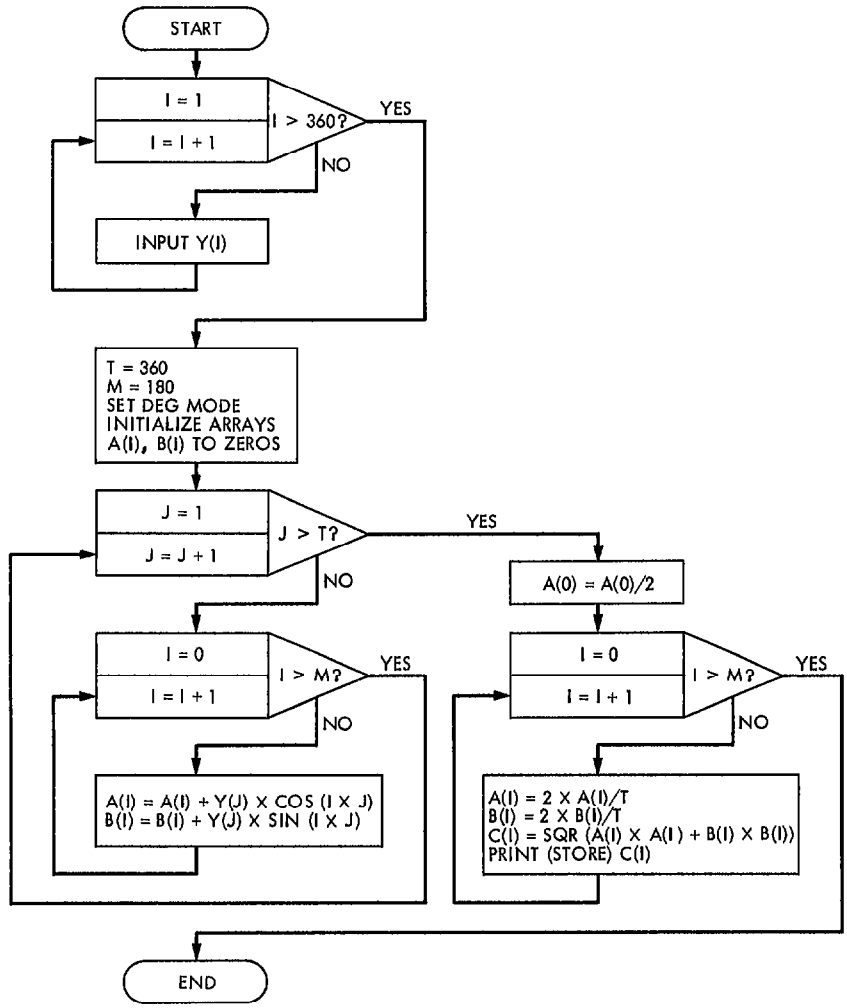

Appendix C

The Set of Film Height Power Spectra

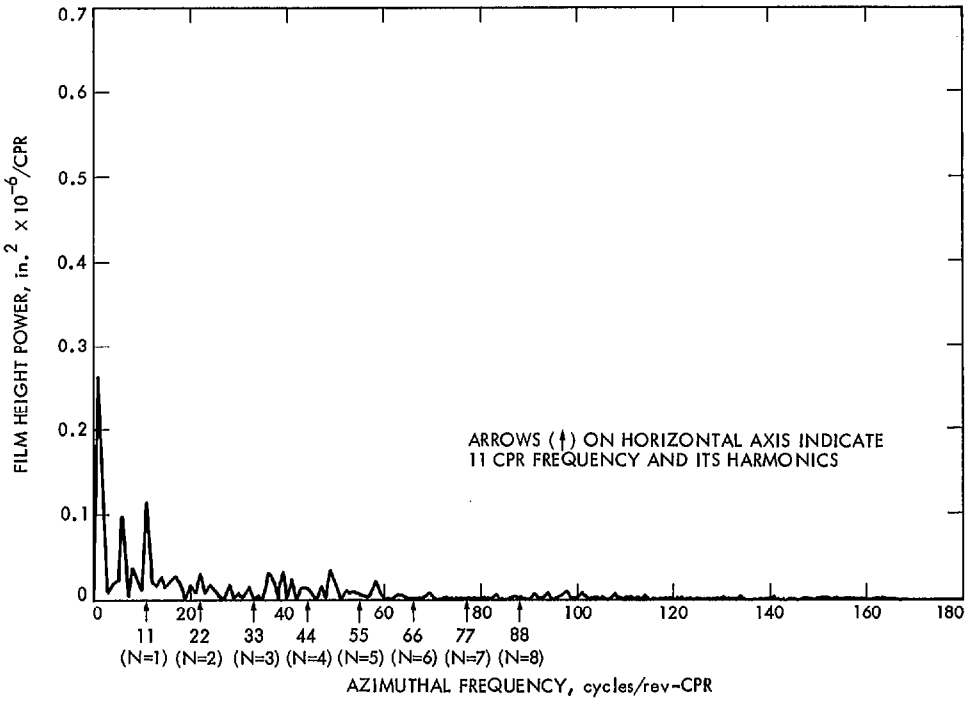

Fig. C-1. Film height power spectrum, right center probe, DSS 14, August 1971

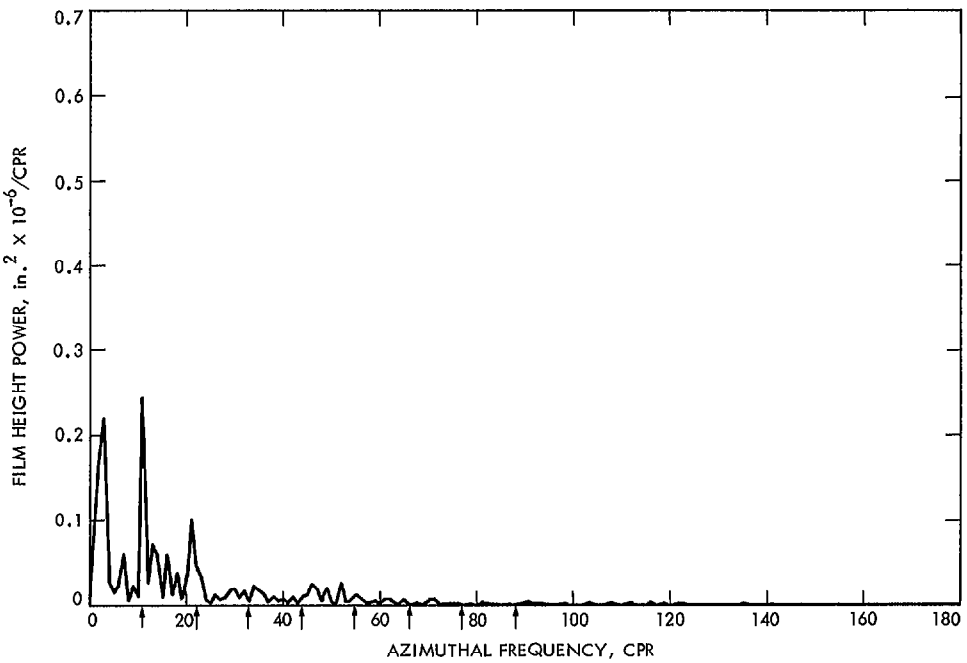

Fig. C-2. Film height power spectrum, right center probe, DSS 14, July 1981

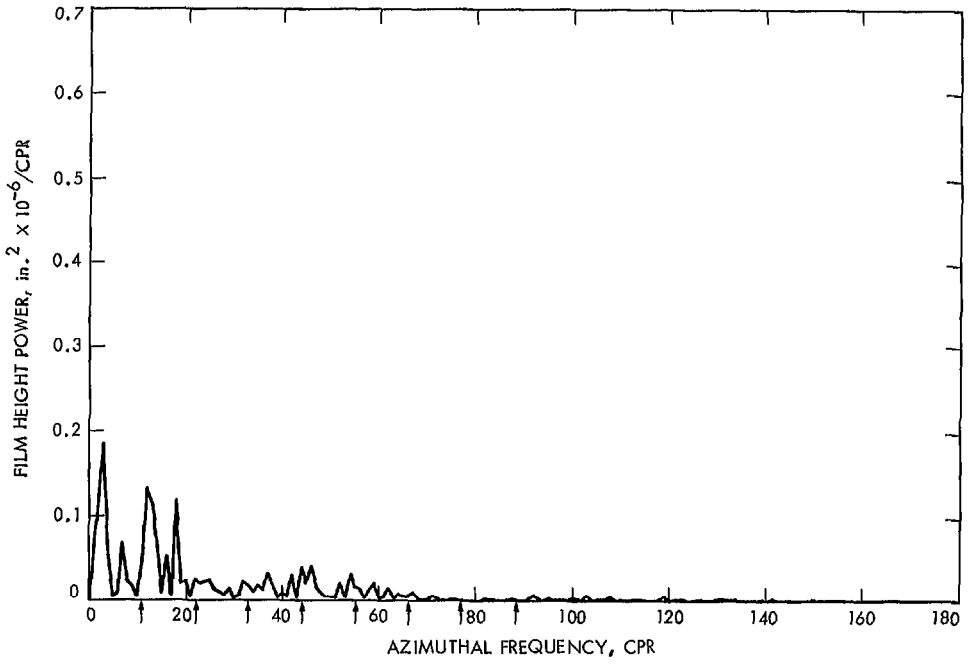

Fig. C-3. Film height power spectrum, right center probe, DSS 14, December 1981

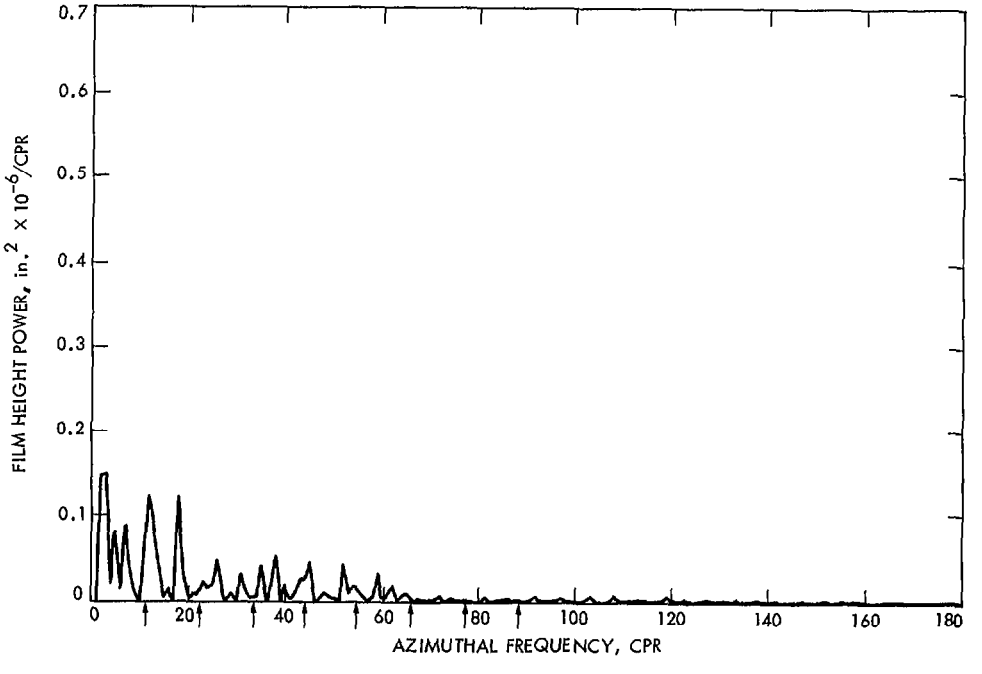

Fig. C-4. Film height power spectrum, right center probe, DSS 14, February 1982

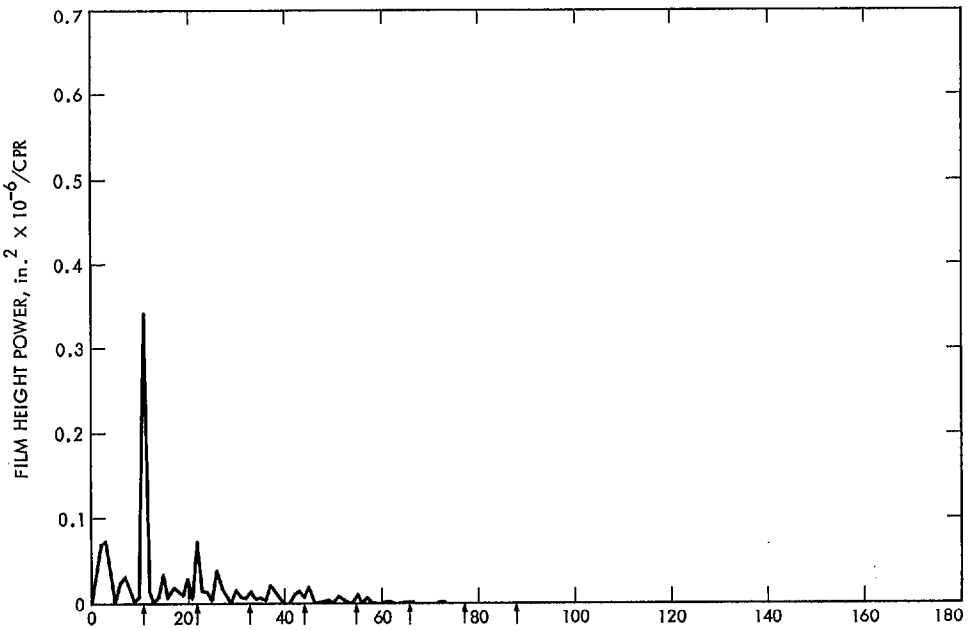

Fig. C-5. Film height power spectrum, right center probe, DSS 43, September 1976

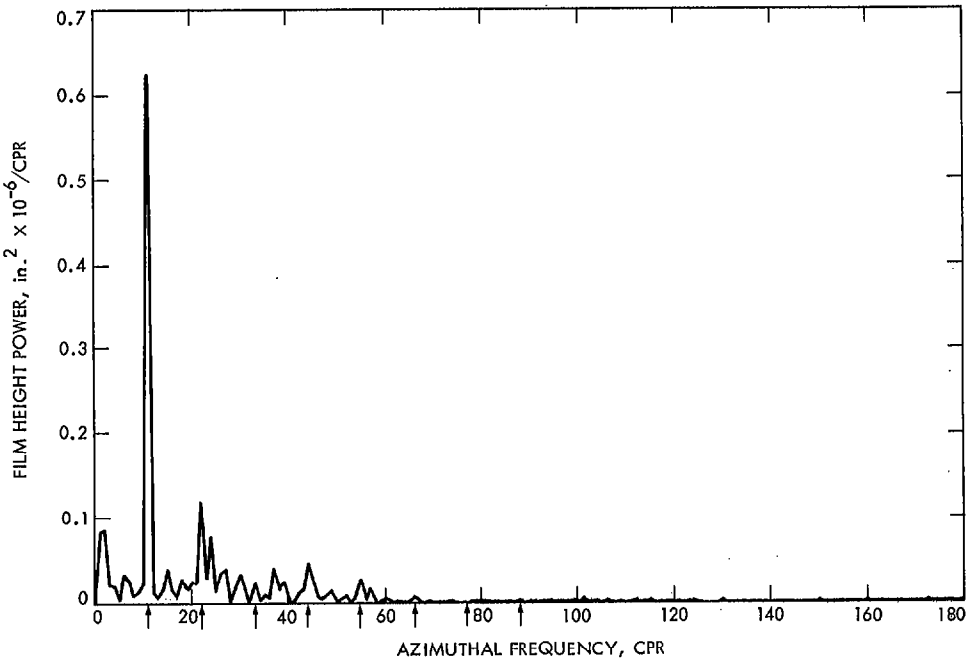

Fig. C-6. Film height power spectrum, right center probe, DSS 43, October 1978

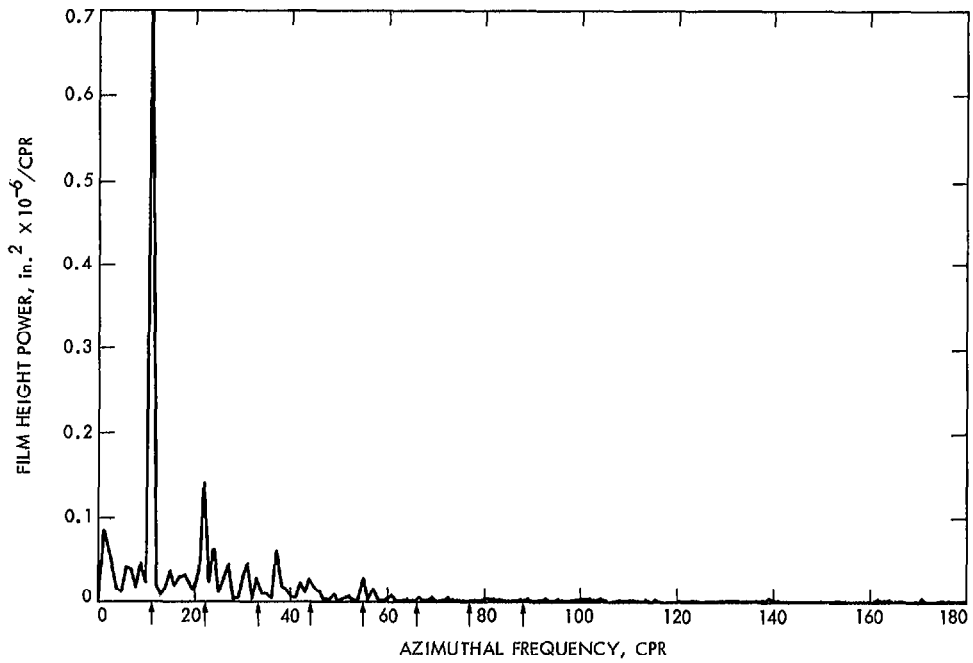

Fig. C-7. Film height power spectrum, right center probe, DSS 43, June 1980

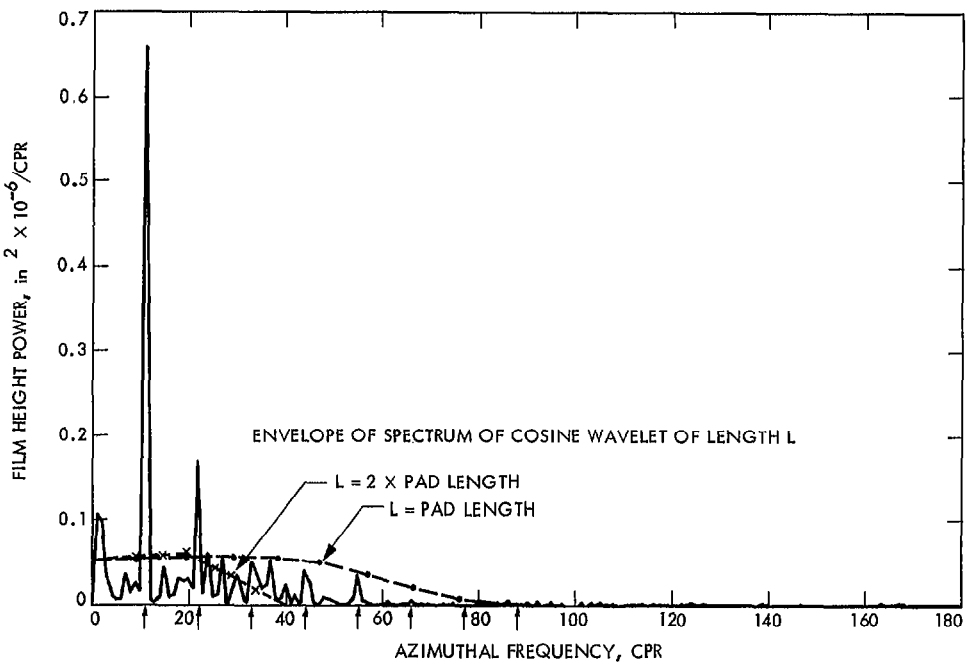

Fig. C-8. Film height power spectrum, right center probe, DSS 43, March 1982

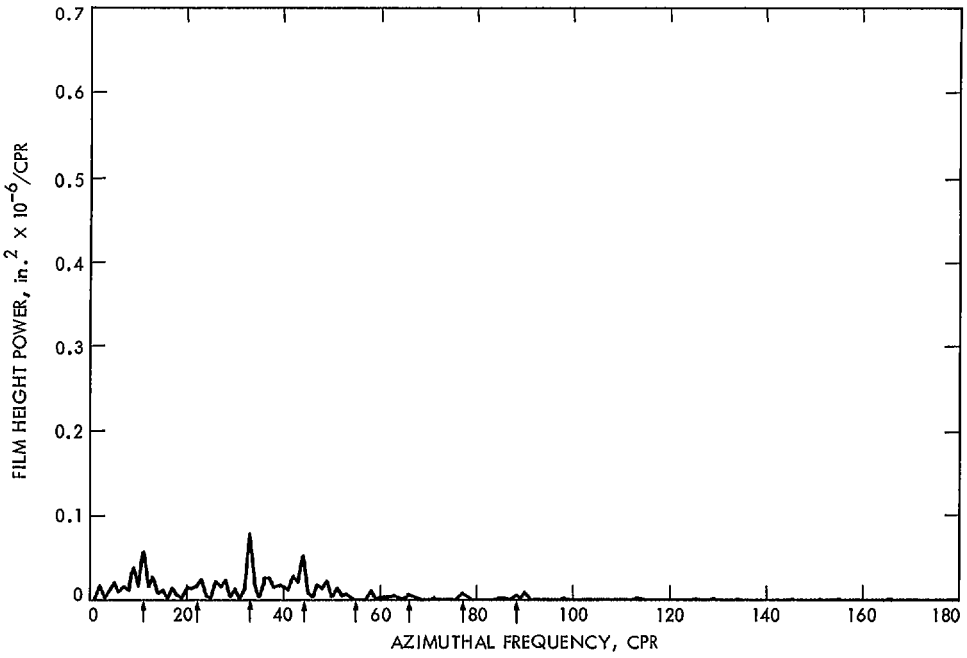

Fig. C-9. Film height power spectrum, right center probe, DSS 63, July 1973

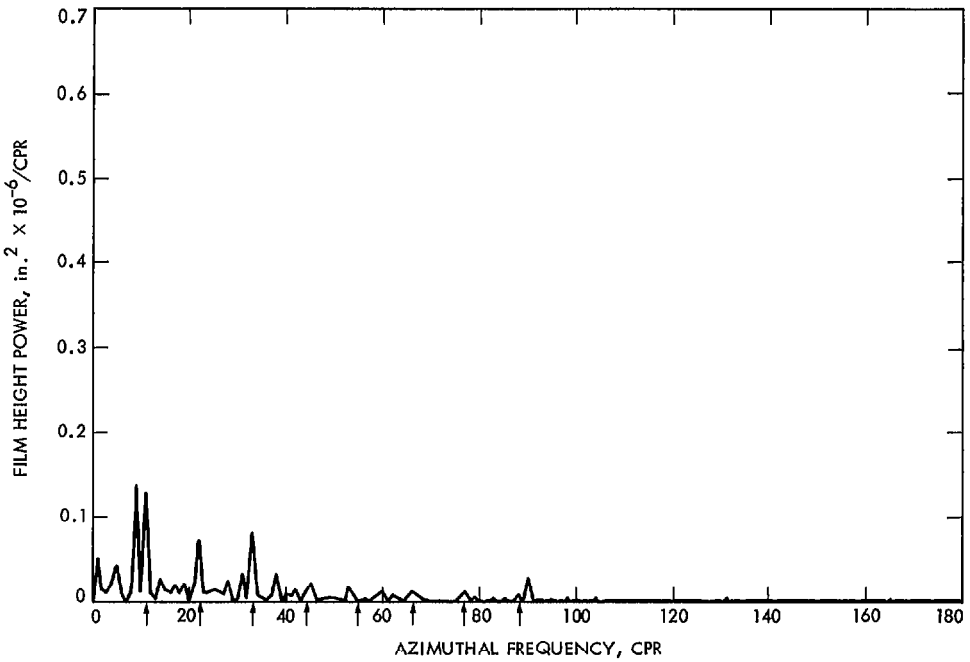

Fig. C-10. Film height power spectrum, right center probe, DSS 63, June 1978

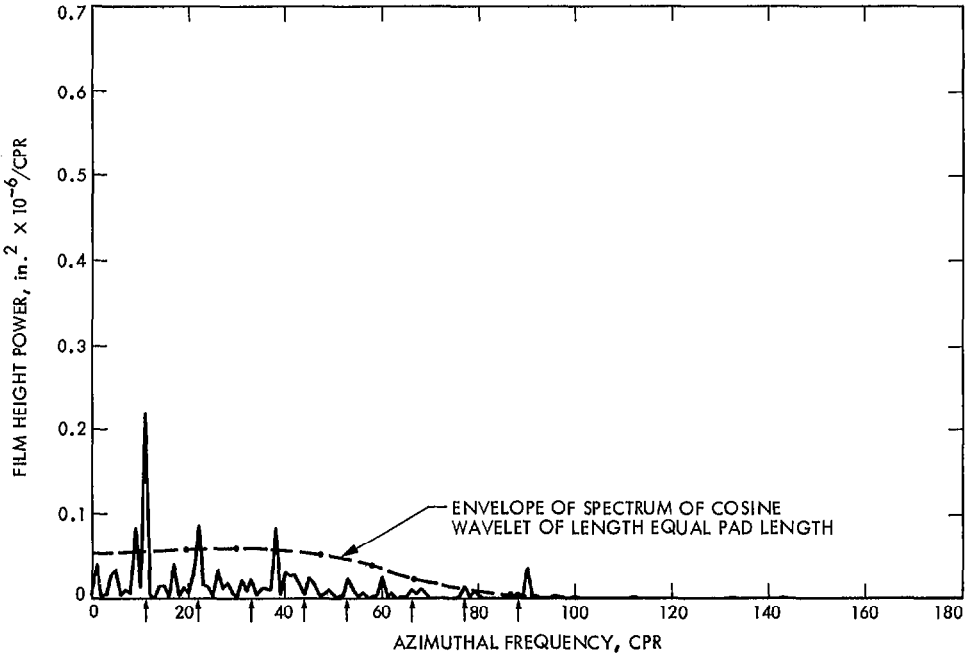

Fig. C-11. Film height power spectrum, right center probe, DSS 63, March 1982